8. K. M. Weltring, B. G. Turgeon, O. C. Yoder, H. D. VanEtten, *Gene* **68**, 335 (1988).
9. V. P. Miao, D. E. Matthews, H. D. VanEtten, *Mol. Gen. Genet.* **226**, 214 (1991).
10. The presence of exclusively 4 Pda^+:4 Pda^- segregation indicates loss of *Pda6* before meiosis in this cross; however, tetrads with 6:2 segregation in other instances of *Pda6* gene loss suggest that this process might also occur during meiosis.
11. G. Chu, D. Vollrath, R. W. Davis, *Science* **234**, 1582 (1986).
12. Progeny from two or three asci collected from each of three perithecia formed by each parent of reciprocal cross 289 (a total of 13 asci) segregated 4 Pda^+:4 Pda^-. Among those examined electrophoretically, asci 2 and 5 were from the same perithecium; asci 1, 3, and 8 were each from a different perithecium.
13. R. N. Jones and H. Rees, *B Chromosomes* (Academic Press, New York, 1982).
14. D. Mills and K. McCluskey, *Mol. Plant-Microbe Interac.* **3**, 351 (1990).
15. M. C. Lucy, P. S. Matthews, H. D. VanEtten, *Physiol. Mol. Plant Pathol.* **33**, 187 (1988).
16. T. Matuo and W. C. Snyder, *Phytopathology* **62**, 731 (1972).
17. W. Schäfer, D. Straney, L. Ciuffetti, H. D. VanEtten, O. C. Yoder, *Science* **246**, 247 (1989).
18. Samples were fractionated in 0.6% agarose at 1.25 V/cm with a 52.5-min pulse time for 140 hours in 89 mM tris, 89 mM boric acid, and 2 mM EDTA at 4°C.
19. Standard techniques for Southern (DNA) analysis were used throughout. J. Sambrook, E. F. Fritsch, T. Maniatis, *Molecular Cloning* (Cold Spring Harbor Laboratory, Cold Spring Harbor, NY, 1989).
20. D. Vollrath, R. W. Davis, C. Connelly, P. Hieter, *Proc. Natl. Acad. Sci. U.S.A.* **85**, 6027 (1988).
21. M. Orbach, D. Vollrath, R. W. Davis, C. Yanofsky, *Mol. Cell. Biol.* **8**, 1469 (1988).
22. Samples were fractionated at 5.7 V/cm with a 100-s pulse time for 20 hours in 0.6% agarose.
23. H. Brody and J. Carbon, *Proc. Natl. Acad. Sci. U.S.A.* **86**, 6260 (1989).
24. The 1.6-Mb chromosome was subjected to pulsed-field electrophoresis in a 0.6% low melting point–agarose gel, then excised, and the gel slices mixed with 1 M NaCl, 25 mM tris (pH 7.5), and 1 mM EDTA. After melting at 70°C, the sample was frozen at −20°C and thawed at 37°C twice. The agarose was removed by centrifugation, and the DNA was precipitated with an equal volume of isopropanol, extracted with phenol-chloroform, and precipitated in ethanol.
25. We thank C. Wasmann and L. Ciuffetti for assistance with figure preparation. Supported in part by a Post Graduate Fellowship from the Natural Science and Research Council of Canada (to V.P.M.), by a National Science Foundation grant awarded (to S.F.C.) in 1990, and by Cooperative State Research Service–United States Department of Agriculture grant 90-37262-5292.

5 July 1991; accepted 24 October 1991

Identification and Characterization of Zinc Binding Sites in Protein Kinase C

STEVAN R. HUBBARD, W. ROBERT BISHOP, PAUL KIRSCHMEIER, SIMON J. GEORGE, STEPHEN P. CRAMER, WAYNE A. HENDRICKSON

Metal ion coordination in the regulatory domain of protein kinase C (PKC) is suggested by the conservation of six cysteines and two histidines in two homologous regions found therein. By monitoring x-ray fluorescence from a purified sample of rat PKC βI overexpressed in insect cells, direct evidence has been obtained that PKC βI tightly binds four zinc ions (Zn^{2+}) per molecule. Extended x-ray absorption fine structure (EXAFS) data are best fit by an average Zn^{2+} coordination of one nitrogen and three sulfur atoms. Of the plausible Zn^{2+} coordination models, only those featuring nonbridged Zn^{2+} sites accommodate the EXAFS data and all of the conserved potential ligands.

PKC IS A CLOSELY RELATED FAMILY of phospholipid-dependent serine/threonine kinases that play a fundamental role in cellular signal transduction (*1*). Nine different mammalian members of the PKC family have been characterized: α, βI, βII, γ, δ, ϵ, ζ [see (*1*) for a review], η (*2*), and L (*3*), and PKC homologs have been identified in *Saccharomyces cerevisiae* (*4*), *Drosophila melanogaster* (*5, 6*), and *Caenorhabditis elegans* (7).

The PKC molecule is a single polypeptide chain containing an NH_2-terminal regulatory domain and a COOH-terminal catalytic domain. The regulatory domain contains the interaction sites of the effector molecules diacylglycerol (DAG), phosphatidylserine, calcium, and tumor-promoting phorbol esters. Within the regulatory domain are two adjacent, highly similar regions of ~50 amino acids containing six conserved cysteines (C) and two conserved histidines (H) in the pattern H-X_{12}-C-X_2-C-X_{10-14}-C-X_2-C-X_4-H-X_2-C-X_7-C (C_6-H_2), where intervening X residues are more variant (Fig. 1). Exceptions to this are the ζ subtype, which contains only one C_6-H_2 region (*8*), and the L subtype, which lacks two of the conserved cysteines and one of the conserved histidines in the second C_6-H_2 region (*3*). The conservation of the six cysteines in these regions was noted early on, but the two equally conserved histidines have received little attention. This C_6-H_2 motif is also found in *n*-chimaerin (*9*), porcine diacylglycerol kinase (*10*), the *unc*-13 gene product (*11*), and the *raf/mil* (*12*) and *vav* (*13*) oncogene products. A study of PKC regulatory domain mutants has shown that the C_6-H_2 regions are essential for the binding of phorbol esters and, by implication, DAG (*14*).

Because PKC is a cytosolic protein and therefore not expected to contain disulfide bonds, a likely function served by this number of conserved cysteines is metal ion coordination. In addition, histidines are common donors of N ligands in Fe, Cu, and Zn ion coordination. The putative ligands, thiolate S and imidazole N atoms, and the absence of color of concentrated PKC solutions suggest Zn^{2+} as a candidate metal ion.

We measured the x-ray fluorescence (XRF) from a purified sample of fully activatable rat PKC βI that had been overexpressed in insect cells (*15*) (Fig. 2A). Synchrotron x-rays were used for excitation, and an energy-discriminating solid-state detector monitored XRF emissions (*16*). We could detect simultaneously a variety of metal ions, from Ca (atomic number $Z = 20$) to Ge ($Z = 32$) by K_α emission and from Sn ($Z = 50$) to Ir ($Z = 77$) by L_α emission.

The XRF data for the PKC βI sample and the control sample, a pool of fractions that eluted just before PKC βI on the last chromatography column, are shown in Fig. 2B. There are three major peaks in common in the two spectra, consistent in energy with Cr and Cu K_α emissions (5.41 and 8.04 keV) and the incident beam scatter (11.2 keV). The Cr and Cu peaks are present in the spectrum of an empty sample cell and are due to trace amounts of those elements in the cell window material. Two peaks are unique to the PKC βI spectrum, consistent with Zn K_α and K_β emissions (8.63 and 9.57 keV). In the difference spectrum (Fig. 2B inset), the Zn K_α and K_β peaks predominate. The significance of the small peak at Cu K_α is unclear. On the basis of a linear regression analysis of Zn standard solutions, the amount of Zn in the PKC βI sample was calculated to be 1.22 ± 0.03 mM. The concentration of PKC βI in the sample was determined by amino acid composition analysis and gel densitometry to be 22.2 ± 1.5 mg/ml (0.29 mM) (*17*). The calculated ratio of Zn^{2+} to PKC βI is thus 4.2 ± 0.3.

The Zn K-edge absorption spectrum for the PKC βI sample is shown in Fig. 3A, and the extracted EXAFS oscillations are shown in Fig. 3B (*18*). EXAFS can provide infor-

S. R. Hubbard and W. A. Hendrickson, Howard Hughes Medical Institute and Department of Biochemistry and Molecular Biophysics, Columbia University, New York, NY 10032.
W. R. Bishop and P. Kirschmeier, Schering-Plough Research, Bloomfield, NJ 07003.
S. J. George, Department of Applied Sciences, University of California, Davis, CA 95616.
S. P. Cramer, Department of Applied Sciences, University of California, Davis, CA 95616, and Division of Applied Science, Lawrence Berkeley Laboratory, Berkeley, CA 94720.

mation on the number and type of ligating atoms and metal-ligand distances (*19*). Initial curve fitting analyses, in which curved wave–derived theoretical backscattering amplitudes and phases computed with the program FEFF (*20*) were used, showed that the observed PKC βI Zn EXAFS is due primarily to backscattering from three to four S atoms at a Zn–S distance of ~2.3 Å (Fig. 3C). Fittings with only three S atoms were significantly improved with the inclusion of an N atom at a Zn–N distance between 2.0 and 2.1 Å (*21*). Curve fitting analyses for several coordination models are given in Table 1. The model consisting of one N and three S atoms (3S/1N) gave the best fit, and the derived Zn–S and Zn–N distances, 2.32 and 2.08 Å, and mean-square deviations are chemically reasonable. In EXAFS analyses, it is generally not possible to determine first shell coordination numbers to better than ~20% (*20*); greater difficulty is encountered for mixed atom–type first shells. Thus, plausible models for Zn^{2+} coordination in PKC βI include at least three and up to four S atoms.

The finding of four Zn^{2+} per PKC βI molecule is consistent with the total number of conserved cysteines and histidines in the two C_6-H_2 regions, 16, and tetracoordination for each Zn^{2+}. There are only two other highly conserved cysteines in the rat PKC βI sequence, and these are found in the catalytic domain. Therefore, the four Zn^{2+} are in all likelihood bound in the C_6-H_2 regions. Given that PKC βI was purified in the continual presence of 1 mM EGTA (dissociation constant K_D for Zn^{2+} is $10^{-12.5}$ M), the Zn^{2+} sites identified are necessarily of high affinity (*22*). These Zn^{2+} evidently serve not as labile regulators of substrate binding but rather as agents that stabilize a particular structural motif. Whether PKC βI contains lower affinity Zn^{2+} sites or whether DAG or phorbol esters directly interact with Zn^{2+} is not addressed in this study.

If the only cysteines involved in Zn^{2+} coordination are the conserved six in each C_6-H_2 region, coordination models that include an average of more than three S atoms per Zn^{2+} will necessarily feature bridged

Fig. 1. Sequence alignment of the two C_6-H_2 regions in the PKC regulatory domain (*32*). (The ζ subtype contains only one region.) The conserved cysteines and histidines are shaded. For the consensus sequence, a capital letter is used if the corresponding residue is found at that position in at least ten (nine) of the eleven (ten) sequences in the first (second) region. A lower-case letter is used if the corresponding residue is found at that position at least six (five) times in the first (second) region. The sequence similarity within a particular subtype across mammalian species is extremely high. For example, the rat and human βI sequences are 98% identical. Sequence references are as follows: rat α, βI/II, γ, δ, ε, and ζ (*8*); mouse η (*2*); human L (*3*); *S. cerevisiae* (*4*); *D. melanogaster* (*5*); and *C. elegans* (*7*).

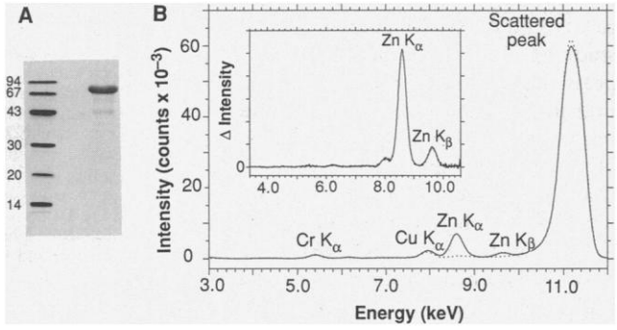

Fig. 2. (**A**) SDS-polyacrylamide gel electrophoresis (12.5%) of the PKC βI sample used for the x-ray experiments (standards are on the left). (**B**) Energy-calibrated XRF spectra of the PKC βI (solid line) and control (dotted line) samples before normalization by incident x-ray flux (effectively the raw data); (inset) normalized difference spectrum.

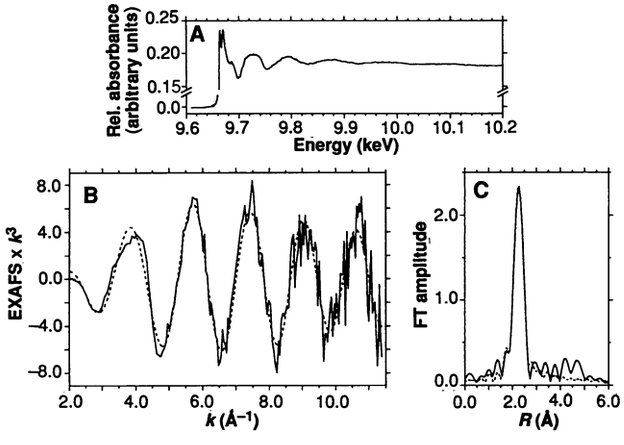

Fig. 3. (**A**) Baseline-subtracted Zn K-edge absorption spectrum for the PKC βI sample. (**B**) Fit of the 3S/1N model (Table 1) to the k^3-weighted, smoothed EXAFS; nonsmoothed experimental spectrum, solid line, and simulated spectrum, dashed line. (**C**) Fourier transform of the experimental and simulated k^3-weighted EXAFS over the k range 2.0 to 11.4 $Å^{-1}$, phase-corrected with Zn–S phases. An R-space window of 1.6 Å approximately centered on the Zn-S peak was used in the backtransformation yielding the first shell to the EXAFS contribution.

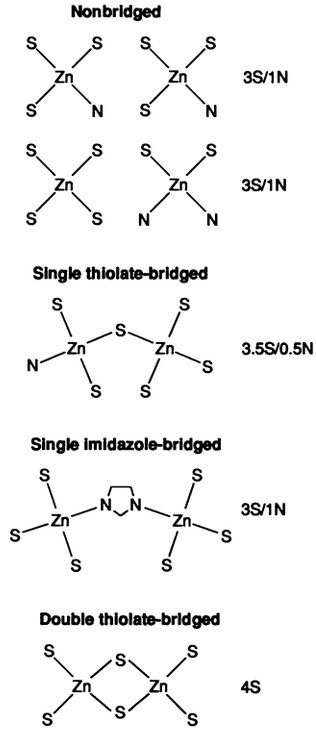

Fig. 4. Candidate models for Zn^{2+} coordination in a PKC C_6-H_2 region consistent with the assumptions given in the text. Except for the bridging ligands, the positions of the S and N ligands with respect to the Zn^{2+} to which they are coordinated are arbitrary. Bond lengths and angles are schematic. The average number of coordinating S and N atoms per Zn^{2+} appears to the right of the models.

Table 1. Results of EXAFS curve fitting analyses for PKC βI. The nonlinear least-squares program OPT (*31*) was used to refine, for each shell, the absorber to backscattering atom distance R and the mean-square deviation σ^2. The single-scattering expression used to compute simulated spectra is given in equation 2 of Rehr *et al.* (*20*). The first values given in the table are from fitting the k^3-weighted, Fourier-filtered EXAFS isolating the first shell contributions, and the values in brackets are from fitting the k^3-weighted, smoothed EXAFS. In the fittings, the overall scale factor was held fixed at 0.9. Adjustments to the threshold energy, ΔE_0, were held fixed at the values derived from the Zn model compound fittings (performed over the same k ranges as the PKC βI fittings). ΔE_0 = −4.2 eV for the Fourier-filtered spectrum fittings (k = 3.0 to 11.0 Å^{-1}) and −6.4 eV for the smoothed spectrum fittings (k = 2.0 to 11.4 Å^{-1}).

Model	Atom	NA*	R (Å)†	σ^2 (Å^2 × 10^3)	Fit index‡
3S/1N	S	3	2.32 [2.31]	3.1 [2.5]	3.1 [144]
	N	1	2.08 [2.03]	2.6 [4.1]	
3.5S/0.5N	S	3.5	2.32 [2.31]	4.2 [3.5]	5.2 [156]
	N	0.5	2.09 [2.00]	1.5 [1.5]	
2S/2S	S	2	2.30 [2.30]	3.1 [10.6]	10.6 [173]
	S	2	2.35 [2.31]	6.2 [1.7]	
4S	S	4	2.32 [2.31]	5.0 [4.7]	11.9 [184]

*The coordination number NA was held fixed during the fittings. †The estimated errors in the distances are ±0.02 Å for Zn–S and ±0.04 Å for Zn–N, based on fittings of the EXAFS spectrum for the Zn model compound in which Zn^{2+} is coordinated by two S and two N atoms. ‡The fit index is defined as $[\Sigma(\chi_e - \chi_s)^2k^6]/n$, where χ_e and χ_s are, respectively, the experimental and simulated EXAFS and n is the number of data points in the fitting range.

Zn^{2+} sites. The possibility of bridging led to a search in the EXAFS data for a Zn–Zn distance in the range 3.0 to 5.0 Å. No evidence was found for a Zn–Zn distance <4 Å, and, although Zn–Zn distances of 4.1 and 4.7 Å were identified, this result is of questionable significance owing to the long distances and the limited data range. Bridging possibilities also motivated an inorganic sulfide analysis of the PKC βI sample; inorganic sulfide often serves as a bridging ligand in metal ion clusters. The result of a colorimetric assay was negative (*23*).

We consider as candidates for the Zn^{2+} sites within a PKC C_6-H_2 region those models that are consistent with the following assumptions: (i) there are two Zn^{2+} sites per C_6-H_2 region; (ii) all six conserved cysteines and either zero, one, or two of the conserved histidines are involved in Zn^{2+} coordination; (iii) the Zn^{2+} are tetracoordinated; and (iv) there is no Zn^{2+} bridging between the two C_6-H_2 regions. The first assumption is derived from our XRF result of four Zn^{2+} per PKC βI molecule and the high sequence similarity between the two C_6-H_2 regions; the second is based on the first shell EXAFS analysis, the absence of inorganic sulfide, and sequence conservation arguments; the third stems from the precedent of tetracoordination in Zn complexes and the EXAFS analysis (*24*); and the fourth comes from the existence of proteins that contain only one copy of the C_6-H_2 motif (*8, 9, 11, 12*).

Models organized according to bridging properties are presented in Fig. 4. The nonbridged models, which are of the 3S/1N type, are the only models in which both conserved histidines donate N ligands. The singly bridged models involve only one of the two conserved histidines, and the doubly bridged model has no role for the histidines. Unfortunately, the EXAFS data do not discriminate completely here. The distance between the single thiolate-bridged Zn^{2+} in the Zn_2Cd_5 metallothionein crystal structure is 3.88 Å (*25*). Judging from an EXAFS study of Zn_7 metallothionein (*26*), it appears that the Zn backscattering contribution in a single thiolate-bridged system is relatively weak. On the basis of the structure of superoxide dismutase (*27*), the Zn–Zn distance in the single imidazole-bridged model is too long to contribute significantly to the EXAFS. From an EXAFS study of GAL4 (*28*), which contains double thiolate-bridged Zn^{2+} (*29*), and the crystal structure of a double thiolate-bridged Zn^{2+} compound (*30*), a prominent peak at ~3.2 Å should be observed in the Fourier transform of the EXAFS for such Zn^{2+} clusters. The absence of such a peak in the PKC βI Fourier transform (Fig. 3C) evidently excludes models featuring doubly bridged Zn^{2+}. Although the EXAFS data do not rule out the singly bridged Zn^{2+} models, only the nonbridged models afford the best fit to the EXAFS and incorporate all of the conserved histidines and cysteines in the C_6-H_2 motif.

REFERENCES AND NOTES

1. Y. Nishizuka, *Nature* **334**, 661 (1988).
2. S.-i. Osada *et al.*, *J. Biol. Chem.* **265**, 22434 (1990).
3. N. Bacher, Y. Zisman, E. Berent, E. Livneh, *Mol. Cell. Biol.* **11**, 126 (1991).
4. D. E. Levin, O. F. Fields, R. Kunisawa, J. M. Bishop, J. Thorner, *Cell* **62**, 213 (1990).
5. A. Rosenthal *et al.*, *EMBO J.* **6**, 433 (1987).
6. E. Schaeffer, D. Smith, G. Mardon, W. Quinn, C. Zuker, *Cell* **57**, 403 (1989).
7. Y. Tabuse, K. Nishiwaki, J. Miwa, *Science* **243**, 1713 (1989).
8. Y. Ono *et al.*, *FEBS Lett.* **226**, 125 (1987).
9. S. Ahmed *et al.*, *Biochem. J.* **272**, 767 (1990).
10. F. Sakane, K. Yamada, H. Kanoh, C. Yokoyama, T. Tanabe, *Nature* **344**, 345 (1990).
11. I. N. Maruyama and S. Brenner, *Proc. Natl. Acad. Sci. U.S.A.* **88**, 5729 (1991).
12. T. I. Bonner *et al.*, *Nucleic Acids Res.* **14**, 1009 (1986); M. Koenen, A. E. Sippel, C. Trachmann, K. Bister, *Oncogene* **2**, 179 (1988).
13. S. Katzav, D. Martin-Zanca, M. Barbacid, *EMBO J.* **8**, 2283 (1989).
14. Y. Ono *et al.*, *Proc. Natl. Acad. Sci. U.S.A.* **86**, 4868 (1989).
15. A baculovirus was constructed for the expression of active PKC βI protein. A clone encoding the full-length βI subtype of rat brain PKC [G. M. Housey *et al.*, *Cell* **52**, 343 (1988)] was cleaved with Bss HII and Hind III; the resulting fragment contained the entire coding region of PKC βI plus ten base pairs of 5′ noncoding sequence. The fragment was blunt-ended with T4 DNA polymerase and ligated to the nonfusion transfer vector pVL941 [V. A. Luckow and M. D. Summers, *Virology* **170**, 31 (1989)] that had been cleaved with Bam HI and blunt-ended as well. Clones were selected and proper orientation was determined by restriction enzyme analysis. Transfer vector DNA was mixed with purified wild-type *Autographa californica* Nuclear Polyhedrosis Virus DNA, prepared according to the methods of M. D. Summers and G. E. Smith [*A Manual of Methods for Baculovirus Vectors and Insect Cell Culture Procedures* (Texas A&M Univ. Press, College Station, 1987)], and transfected onto Sf-9 cells (obtained from the American Type Culture Collection) grown in supplemented Grace's medium (GIBCO). After 6 days the supernatant was harvested, and recombinant virus was purified from wild-type virus by limiting dilution and dot-hybridization (M. D. Summers and G. E. Smith, *ibid.*). Final recombinant viruses were selected by screening for their ability to express PKC βI in infected cells. At 72 hours after infection, Sf-9 cells were harvested by centrifugation at 12,000*g* and homogenized in buffer containing 20 mM tris-HCl (pH 7.5), 10 mM EGTA, 15 mM 2-mercaptoethanol, leupeptin (10 μg/ml), phenylmethylsulfonyl fluoride (PMSF) (40 μg/ml), soybean trypsin inhibitor (10 μg/ml), and 0.1% Triton X-100. PKC βI was purified in three chromatographic steps: DEAE-Sephacel (Pharmacia-LKB) and phenyl-Sepharose (CL-4B, Pharmacia-LKB) [T. Kitano, M. Go, U. Kikkawa, Y. Nishizuka, *Methods Enzymol.* **124**, 349 (1986)], and hydroxylapatite (Bio-Gel HPHT, BioRad) [M. S. Shearman, K. Ogita, U. Kikkawa, Y. Nishizuka, *ibid.* **168**, 347 (1989)]; the DEAE-Sephacel buffer included leupeptin (10 μg/ml) and PMSF (40 μg/ml), and in each column buffer 1 mM EGTA was included instead of 0.5 mM EGTA and 0.5 mM EDTA. PKC βI activity was assayed as described by C. A. O'Brian, D. A. Lawrence, E. T. Kaiser, and I. B. Weinstein [*Biochem. Biophys. Res. Commun.* **124**, 296 (1984)], except that histone III-S was used as the phosphoacceptor. Typically, this protocol yielded between 0.6 and 1.8 mg of purified PKC βI per liter of cell culture with a specific activity of between 447 and 637 nmol/mg per minute. For the x-ray experiments, PKC βI from three different preparations was pooled and concentrated in Centricon-30 microconcentrators (Amicon).
16. Data were collected at the National Synchrotron Light Source, Brookhaven National Laboratory, on beam line X-19A equipped with a Si (220) double-crystal monochromator tuned to an energy of 11.2 keV. Pulse height analysis was performed on the amplified output of one of the 13 Ge elements of the detector array [S. P. Cramer, O. Tench, M. Yocum, G. N. George, *Nucl. Instrum. Methods A* **266**, 586 (1988)] with a Canberra multichannel analyzer (MCA). A Lucite cell (23.1 mm by 3.2 mm by 0.8 mm) was used for the XRF and EXAFS experi-

ments; thin Mylar tape was used for the one window. Fluorescence was monitored in the direction normal to the incident x-ray beam in the horizontal plane. A single sample cell, extensively rinsed with an EDTA solution and deionized water between samples, was used for all the XRF measurements. Zn standards of 0, 0.5, 1.0, and 2.0 mM were prepared from a Zn atomic absorption standard solution (Sigma); solution volumes were measured gravimetrically. Data for the PKC βI and control samples and the Zn standard solutions were accumulated for 5 min each at room temperature. Raw data in the form of fluorescence counts versus MCA channel number were converted to counts versus energy with the Cr K_α peak (5.41 keV) and the scatter peak (11.2 keV) in a two-point linear calibration. Each of the energy-calibrated spectra was interpolated onto an evenly spaced energy grid and normalized by the integrated counts in the scatter peak to correct for differences in total incident flux. Difference spectra were computed for the Zn standards and the PKC βI sample (PKC βI − control), and the counts in the Zn K_α peaks were integrated. The standard deviation for the Zn concentration in the PKC βI sample was estimated from the results of different attempts at energy calibration, spectra normalization, and integration of the Zn counts.

17. The composition analysis, for which duplicate measurements were made on two different sample aliquots, gave a value of 29.2 ± 1.2 mg/ml for the total protein concentration. Coomassie blue–stained SDS-polyacrylamide gels (12.5%) (Fig. 2A) were scanned (two dimensionally) with a Molecular Dynamics densitometer to obtain an estimate of the percentage of protein that was PKC βI. Several lanes with differing amounts of loaded protein were analyzed. The PKC βI band comprised 76 ± 4% of the total stained protein. The next highest intensity band was ~4% of the total.
18. Fluorescence EXAFS data for the PKC βI sample were taken at ~15 K. Twenty-one scans, each 35 min in duration, were recorded with step sizes of 2.0 and 3.0 eV in the EXAFS region. Because of a small amount of contaminating W in the He cryostat, the usable data range was limited to <10.2 keV. Two scans to be used for baseline subtraction were taken of the cell containing sample buffer. The monochromator crystals were detuned to 42% to suppress higher energy harmonics. A Zn foil placed downstream of the sample position was used to calibrate the energy; 9.661 keV was assigned to the K-edge inflection point. Averaged sample spectra were computed; the data from each Ge element of the detector array were weighted by the size of the edge jump. The baseline spectrum showed a small Zn K-edge feature (edge jump was 14% of that of the PKC βI sample) due to a contaminant in the cryostat. The baseline spectrum was smoothed, retaining the edge feature, and subtracted from the PKC βI spectrum. A cubic spline was fit to the region above the edge to extract the EXAFS oscillations. Conversion from energy E (keV) to photoelectron wave number k ($Å^{-1}$) was done with an estimate for the threshold energy, E_0, of 9.670 keV [$k = \sqrt{0.262(E-E_0)}$]. EXAFS spectra were smoothed with a Gaussian function of width 0.1 $Å^{-1}$. Transmission EXAFS data for a Zn model compound, (1,10-phenanthroline)bis(4-toluenethiolato)Zn^{2+} [T. L. Cremers, D. R. Bloomquist, R. D. Willet, G. A. Crosby, *Acta Crystallogr. B* **36**, 3097 (1980)], in the form of a sucrose-diluted fine powder, were taken at room temperature.
19. S. P. Cramer and K. O. Hodgson, *Prog. Inorg. Chem.* **25**, 1 (1979).
20. J. J. Rehr, J. Mustre de Leon, S. I. Zabinsky, R. C. Albers, *J. Am. Chem. Soc.* **113**, 5135 (1991).
21. Discriminating between an N and an O backscatterer is difficult, especially when the contribution of the low-Z ligand to the EXAFS is minor. In favorable cases, the backscattering contributions (from single and multiple scattering) from the outer C and N atoms of the His imidazole group are clearly observable [S. S. Hasnain and R. W. Strange, in *Synchrotron Radiation and Biophysics*, S. S. Hasnain, Ed. (Wiley, New York, 1990), chap. 4]. The analysis program EXCURV90 [N. Binstead, J. W. Campbell, S. J. Gurman, P. C. Stephenson, *SERC Daresbury Laboratory EXCURV90 Program* (1990)] was used to simulate single and multiple-scattering contributions from a single imidazole among three S backscatterers. The results indicated that the outer shell imidazole contributions would likely be obscured in experimental data.
22. In an initial XRF experiment with a less pure and less concentrated PKC βI sample, isolated in the presence of 0.5 mM EGTA and 0.5 mM EDTA (K_D for Zn^{2+} is $10^{-16.4}$ M), a Zn^{2+} to PKC βI stoichiometry of 3.1 ± 0.7 was obtained. We conclude from the two XRF results that in the presence of 1 mM EGTA all of the high affinity Zn^{2+} sites are loaded.
23. An assay to detect the presence of inorganic sulfide was performed according to the procedures of T. E. King and R. O. Morris [*Methods Enzymol.* **10**, 634 (1967)]. Using sodium sulfide and red algae ferredoxin (Sigma) as standards, we determined the amount of sulfide in the PKC βI sample to be <0.1 mol per mol of PKC βI.
24. Although pentacoordination by S and N atoms is found in bioinorganic Zn^{2+} compounds, in those cases examined one or more Zn–S distances are longer than the average Zn–S distance by at least 0.25 Å [T. P. E. Auf der Heyde and L. R. Nassimbeni, *Acta Crystallogr. B* **40**, 582 (1984)]. No evidence for a long S ligand is found in the EXAFS data.
25. A. H. Robbins *et al.*, *J. Mol. Biol.* **221**, 1269 (1991).
26. S. S. Hasnain *et al.*, *Experientia Suppl.* **52**, 227 (1987).
27. J. A. Tainer, E. D. Getzoff, K. M. Beem, J. S. Richardson, D. C. Richardson, *J. Mol. Biol.* **160**, 181 (1982).
28. J. F. Povey, G. P. Diakun, C. D. Garner, S. P. Wilson, E. D. Laue, *FEBS Lett.* **266**, 142 (1990).
29. T. Pan and J. E. Coleman, *Biochemistry* **29**, 3023 (1990).
30. A. D. Watson, C. P. Rao, J. R. Dorfman, R. H. Holm, *Inorg. Chem.* **24**, 2820 (1985).
31. T. K. Eccles, thesis, Stanford University (1977); modifications to the program were made by G. N. George (Exxon Research) and S.P.C.
32. Single-letter abbreviations for the amino acid residues are as follows: A, Ala; C, Cys; D, Asp; E, Glu; F, Phe; G, Gly; H, His; I, Ile; K, Lys; L, Leu; M, Met; N, Asn; P, Pro; Q, Gln; R, Arg; S, Ser; T, Thr; V, Val; W, Trp; and Y, Tyr.
33. We gratefully acknowledge J. Petrin's role in the PKC βI purification and the contributions of G. M. Housey and I. B. Weinstein to the cloning and overexpression of PKC βI. We benefited from discussions with G. N. George, R. A. Scott, B. Hedman, and K. O. Hodgson on EXAFS matters, and we thank W. Orme-Johnson for helpful suggestions on the inorganic sulfide assay. The Zn model compound was kindly provided by G. A. Crosby.

29 August 1991; accepted 30 October 1991

Novel Fold and Putative Receptor Binding Site of Granulocyte-Macrophage Colony-Stimulating Factor

KAY DIEDERICHS, TOM BOONE, P. ANDREW KARPLUS*

Granulocyte-macrophage colony-stimulating factor (GM-CSF) stimulates the development of and the cytotoxic activity of white blood cells. Recombinant human GM-CSF has proven useful in the treatment of blood disorders. The structure of GM-CSF, which was determined at 2.4 angstrom resolution by x-ray crystallography, has a novel fold combining a two-stranded antiparallel β sheet with an open bundle of four α helices. Residues implicated in receptor recognition, which are distant in the primary sequence, are on adjacent α helices in the folded protein. A working model for the receptor binding site is presented.

NATURAL GM-CSF IS A 127–AMINO acid residue trace glycoprotein (*1, 2*) that triggers the development of both granulocyte and macrophage colonies from hematopoietic progenitor cells (*3*). The availability of recombinant GM-CSF (*2, 4, 5*) has allowed a much fuller characterization of its activities, and it is now clear that GM-CSF stimulates a wide variety of hematopoietic and nonhematopoietic cell types (*6*). As a therapeutic agent, GM-CSF has shown promise in the treatment of aplastic anemia, myelodysplastic syndromes, acquired immune deficiency syndrome, neutropenias, and chemotherapy-induced myelosuppression (*7, 8*). As a step toward understanding its structure-function relations, we have crystallized nonglycosylated recombinant human GM-CSF (*9*). Here we report the structure at 2.4 Å resolution and define a putative receptor binding site.

The tertiary structure of GM-CSF is dominated by a bundle of four α helices and is distinctly nonspherical with dimensions of 20 Å by 30 Å by 40 Å (Fig. 1). The four helices are all antiparallel and form a twisted open barrel, with the open edge filled in by strand 1 of the antiparallel sheet. Each of the helices interacts with both of its neighbors around the barrel perimeter (Table 1) so that despite the presence of the β sheet, GM-CSF can be compared with known four-helix bundle proteins (*10*). The topology of the bundle places helices A and B, and helices C and D across the barrel from each other rather than next to each other. This placement gives GM-CSF a double overhand topology (*10*), which has previously been seen for porcine growth hormone (*11*). Although interesting, the simi-

K. Diederichs and P. A. Karplus, Section of Biochemistry, Molecular and Cell Biology, Cornell University, Ithaca, NY 14853.
T. Boone, AMGEN, Thousand Oaks, CA 91320–1789.

*To whom correspondence should be addressed.